Arbitrary waveform generator and differentiator employing an integrated optical pulse shaper

Shasha Liao,[1] Yunhong Ding,[2] Jianji Dong,[1,*] Ting Yang,[1] Xiaolin Chen,[1] Dingshan Gao,[1,3] and Xinliang Zhang[1]

[1]*Wuhan National Laboratory for Optoelectronics, School of Optoelectronic Science and Engineering, Huazhong University of Science and Technology, Wuhan, 43007, China*
[2]*Department of Photonics Engineering, Technical University of Denmark, 2800 Kgs. Lyngby, Denmark*
[3]*State Key Laboratory on Integrated Optoelectronics, College of Electronic Science and Engineering, Jilin University, Changchun 130012, China*
[*]*jjdong@mail.hust.edu.cn*

Abstract: We propose and demonstrate an optical arbitrary waveform generator and high-order photonic differentiator based on a four-tap finite impulse response (FIR) silicon-on-insulator (SOI) on-chip circuit. Based on amplitude and phase modulation of each tap controlled by thermal heaters, we obtain several typical waveforms such as triangular waveform, sawtooth waveform, square waveform and Gaussian waveform, etc., assisted by an optical frequency comb injection. Unlike other proposed schemes, our scheme does not require a spectral disperser which is difficult to fabricate on chip with high resolution. In addition, we demonstrate first-, second- and third-order differentiators based on the optical pulse shaper. Our scheme can switch the differentiator patterns from first- to third-order freely. In addition, our scheme has distinct advantages of compactness, capability for integration with electronics.

OCIS codes: (070.1170) Analog optical signal processing; (200.0200) Optics in computing; (130.3120) Integrated optics devices; (320.5540) Pulse shaping.

References and links

1. X. Fang, D. N. Wang, and S. Li, "Fiber Bragg grating for spectral phase optical code-division multiple-access encoding and decoding," J. Opt. Soc. Am. B **20**(8), 1603–1610 (2003).
2. A. M. Weiner, "Ultrafast optical pulse shaping: A tutorial review," Opt. Commun. **284**(15), 3669–3692 (2011).
3. A. Monsterleet, S. Tonda-Goldstein, D. Dolfi, J. Huignard, P. Sapé, and J. Chazelas, "Optically generated arbitrary waveforms for radar applications," Electron. Lett. **41**(6), 332–334 (2005).
4. J. Dong, B. Luo, Y. Zhang, L. Lei, D. Huang, and X. Zhang, "All-optical temporal differentiator using a high resolution optical arbitrary waveform shaper," Chin. Phys. Lett. **29**(1), 014203 (2012).
5. A. Zheng, J. Dong, L. Lei, T. Yang, and X. Zhang, "Diversity of photonic differentiators based on flexible demodulation of phase signals," Chin. Phys. B. **23**(3), 033201 (2014).
6. F. M. Kuo, J. W. Shi, H. C. Chiang, H. P. Chuang, H. K. Chiou, C. L. Pan, N. W. Chen, H. J. Tsai, and C. B. Huang, "Spectral power enhancement in a 100 GHz photonic millimeter-wave generator enabled by spectral line-by-line pulse shaping," IEEE Photon. J. **2**(5), 719–727 (2010).
7. C. Wang and J. Yao, "Large time-bandwidth product microwave arbitrary waveform generation using a spatially discrete chirped fiber Bragg grating," J. Lightwave Technol. **28**(11), 1652–1660 (2010).
8. A. Zhang and C. Li, "Dynamic optical arbitrary waveform generation with amplitude controlled by interference of two FBG arrays," Opt. Express **20**(21), 23074–23081 (2012).
9. B. Bortnik, I. Y. Poberezhskiy, J. Chou, B. Jalali, and H. R. Fetterman, "Predistortion technique for RF-photonic generation of high-power ultrawideband arbitrary waveforms," J. Lightwave Technol. **24**(7), 2752–2759 (2006).
10. C. B. Huang, D. E. Leaird, and A. M. Weiner, "Time-multiplexed photonically enabled radio-frequency arbitrary waveform generation with 100 ps transitions," Opt. Lett. **32**(22), 3242–3244 (2007).
11. Y. Dai, X. Chen, H. Ji, and S. Xie, "Optical arbitrary waveform generation based on sampled fiber Bragg gratings," IEEE Photon. Technol. Lett. **19**(23), 1916–1918 (2007).
12. J. Yao, "Photonics for ultrawideband communications," IEEE Microw. Mag. **10**(4), 82–95 (2009).
13. D. J. Geisler, N. K. Fontaine, T. He, R. P. Scott, L. Paraschis, J. P. Heritage, and S. J. Yoo, "Modulation-format agile, reconfigurable Tb/s transmitter based on optical arbitrary waveform generation," Opt. Express **17**(18), 15911–15925 (2009).

#236566 - $15.00 USD Received 19 Mar 2015; revised 24 Apr 2015; accepted 27 Apr 2015; published 29 Apr 2015

14. W. Jiang, F. M. Soares, S. W. Seo, J. H. Baek, N. K. Fontaine, R. G. Broeke, J. Cao, J. Yan, K. Okamoto, and F. Olsson, "A monolithic InP-based photonic integrated circuit for optical arbitrary waveform generation, " in *National Fiber Optic Engineers Conference* (Optical Society of America, 2008), p. JThA39.
15. A. Politi, M. J. Cryan, J. G. Rarity, S. Yu, and J. L. O'Brien, "Silica-on-silicon waveguide quantum circuits," Science **320**(5876), 646–649 (2008).
16. Y. Okawachi, K. Saha, J. S. Levy, Y. H. Wen, M. Lipson, and A. L. Gaeta, "Octave-spanning frequency comb generation in a silicon nitride chip," Opt. Lett. **36**(17), 3398–3400 (2011).
17. F. Ferdous, H. Miao, D. E. Leaird, K. Srinivasan, J. Wang, L. Chen, L. T. Varghese, and A. M. Weiner, "Spectral line-by-line pulse shaping of on-chip microresonator frequency combs," Nat. Photonics **5**(12), 770–776 (2011).
18. F. Ferdous, H. Miao, P. H. Wang, D. E. Leaird, K. Srinivasan, L. Chen, V. Aksyuk, and A. M. Weiner, "Probing coherence in microcavity frequency combs via optical pulse shaping," Opt. Express **20**(19), 21033–21043 (2012).
19. M. H. Khan, H. Shen, Y. Xuan, L. Zhao, S. Xiao, D. E. Leaird, A. M. Weiner, and M. Qi, "Ultrabroad-bandwidth arbitrary radiofrequency waveform generation with a silicon photonic chip-based spectral shaper," Nat. Photonics **4**(2), 117–122 (2010).
20. R. Slavík, Y. Park, N. Ayotte, S. Doucet, T. J. Ahn, S. LaRochelle, and J. Azaña, "Photonic temporal integrator for all-optical computing," Opt. Express **16**(22), 18202–18214 (2008).
21. T. Yang, J. Dong, S. Liao, D. Huang, and X. Zhang, "Comparison analysis of optical frequency comb generation with nonlinear effects in highly nonlinear fibers," Opt. Express **21**(7), 8508–8520 (2013).
22. S. Liao, S. Min, and J. Dong, "On-chip optical pulse shaper for arbitrary waveform generation using optical gradient force, " in *Optical Communication (ECOC), 2014 European Conference on*(IEEE, 2014), pp. 1–3.
23. N. K. Fontaine, R. P. Scott, J. Cao, A. Karalar, W. Jiang, K. Okamoto, J. P. Heritage, B. H. Kolner, and S. J. Yoo, "32 phase× 32 amplitude optical arbitrary waveform generation," Opt. Lett. **32**(7), 865–867 (2007).
24. R. P. Scott, N. K. Fontaine, C. Yang, D. J. Geisler, K. Okamoto, J. P. Heritage, and S. J. Yoo, "Rapid updating of optical arbitrary waveforms via time-domain multiplexing," Opt. Lett. **33**(10), 1068–1070 (2008).
25. A. Dezfooliyan and A. M. Weiner, "Photonic synthesis of high fidelity microwave arbitrary waveforms using near field frequency to time mapping," Opt. Express **21**(19), 22974–22987 (2013).
26. A. Vega, D. E. Leaird, and A. M. Weiner, "High-speed direct space-to-time pulse shaping with 1 ns reconfiguration," Opt. Lett. **35**(10), 1554–1556 (2010).
27. C. Wang and J. Yao, "Photonic generation of chirped millimeter-wave pulses based on nonlinear frequency-to-time mapping in a nonlinearly chirped fiber Bragg grating," IEEE Trans. Microw. Theory Tech. **56**(2), 542–553 (2008).
28. S. Liao, Y. Ding, C. Peucheret, T. Yang, J. Dong, and X. Zhang, "Integrated programmable photonic filter on the silicon-on-insulator platform," Opt. Express **22**(26), 31993–31998 (2014).
29. C. Madsen, G. Lenz, A. Bruce, M. Cappuzzo, L. Gomez, and R. Scotti, "Integrated all-pass filters for tunable dispersion and dispersion slope compensation," IEEE Photon. Technol. Lett. **11**(12), 1623–1625 (1999).
30. G. Lenz, B. Eggleton, C. K. Madsen, and R. Slusher, "Optical delay lines based on optical filters," IEEE J. Quantum Electron. **37**(4), 525–532 (2001).
31. Y. Park, M. H. Asghari, T. J. Ahn, and J. Azaña, "Transform-limited picosecond pulse shaping based on temporal coherence synthesization," Opt. Express **15**(15), 9584–9599 (2007).
32. A. Zheng, T. Yang, X. Xiao, Q. Yang, X. Zhang, and J. Dong, "Tunable fractional-order differentiator using an electrically tuned silicon-on-isolator Mach-Zehnder interferometer," Opt. Express **22**(15), 18232–18237 (2014).
33. J. Dong, A. Zheng, D. Gao, S. Liao, L. Lei, D. Huang, and X. Zhang, "High-order photonic differentiator employing on-chip cascaded microring resonators," Opt. Lett. **38**(5), 628–630 (2013).
34. R. A. Soref, "Silicon-based optoelectronics," Proc. IEEE **81**(12), 1687–1706 (1993).
35. N. N. Feng, P. Dong, D. Feng, W. Qian, H. Liang, D. C. Lee, J. B. Luff, A. Agarwal, T. Banwell, R. Menendez, P. Toliver, T. K. Woodward, and M. Asghari, "Thermally-efficient reconfigurable narrowband RF-photonic filter," Opt. Express **18**(24), 24648–24653 (2010).
36. Y. Ding, H. Ou, and C. Peucheret, "Ultrahigh-efficiency apodized grating coupler using fully etched photonic crystals," Opt. Lett. **38**(15), 2732–2734 (2013).
37. Y. Ding, C. Peucheret, H. Ou, and K. Yvind, "Fully etched apodized grating coupler on the SOI platform with–0.58 dB coupling efficiency," Opt. Lett. **39**(18), 5348–5350 (2014).
38. J. Azaña, "Ultrafast analog all-optical signal processors based on fiber-grating devices," IEEE Photon. J. **2**(3), 359–386 (2010).
39. M. Li, L. Y. Shao, J. Albert, and J. Yao, "Continuously tunable photonic fractional temporal differentiator based on a tilted fiber Bragg grating," IEEE Photon. Technol. Lett. **23**(4), 251–253 (2011).
40. K. A. Rutkowska, D. Duchesne, M. J. Strain, R. Morandotti, M. Sorel, and J. Azaña, "Ultrafast all-optical temporal differentiators based on CMOS-compatible integrated-waveguide Bragg gratings," Opt. Express **19**(20), 19514–19522 (2011).

1. Introduction

Optical arbitrary waveform generation (OAWG) plays a critical role in many applications, such as generating optical ultra-wide band (UWB) signal [1, 2], optical pulse radar [3], all-optical temporal differentiator [4, 5], and test of optical communication system. Although lots of OAWG schemes were reported using mature fiber grating techniques [2, 6–12], one of the

#236566 - $15.00 USD Received 19 Mar 2015; revised 24 Apr 2015; accepted 27 Apr 2015; published 29 Apr 2015

most promising solutions is prone to be the miniaturization and integration with photonic integrated circuits, such as using indium phosphide (InP) platform [13, 14], silica on silicon [15], silicon nitride [16–18] or silicon platform [19, 20]. To generate arbitrary waveform in optical domain, one needs a source of optical frequency comb [21] and an optical pulse shaper [22]. The pulse shaper consists of a spectral disperser to separate the frequency comb line by line, complex modulator array, and an opposite spectral disperser to combine these frequency lines. S. J. B. Yoo *et al* presented an integrated array waveguide grating scheme in InP and silicon platforms, respectively [23, 24]. These schemes showed very excellent performances, with compact size and very low power consumption. However, it is still difficult to manipulate the comb lines one by one in integrated spectral disperser when the comb spacing is very small. It is a big challenge for the chip fabrication with high resolution. Another feasible solution is to design a reconfigurable whole spectral function and then use fiber dispersion to form a temporal function with frequency-to-time mapping [25–27]. But in fact, the on-chip mapping device with adequate large dispersion is very difficult to achieve. In our previous work, we have demonstrated a programmable optical filter with integrated silicon platform, which is based on four-tap FIR structure [28]. This structure is widely used in many aspects, such as dispersion compensation [29] and time delay [30]. And this structure can be regarded as an optical pulse shaper and the principle is similar to the scheme presented by Yongwoo Park *et al*. in 2007 [31]. Comparing to previous pulse shaper, the chip fabrication is very simple and no spectral disperser is required.

In this paper, we further demonstrate an OAWG and high-order photonic differentiator based on a four-tap FIR silicon integrated circuit. By thermally controlling the amplitude and phase of each tap, we obtain several typical waveforms such as triangular waveform, sawtooth waveform, square waveform and Gaussian waveform, etc. Furthermore, we demonstrate first-, second- and third-order differentiation based on the optical pulse shaper, whose spectra were tailored to the transfer functions of temporal differentiators. Especially, our scheme can switch the differentiator patterns from first- to third-order freely on a fixed photonic chip, and this is unable in our previous works such as cascaded microrings or cascaded Mach-Zehnder interferometers (MZIs) [32, 33]. Moreover, our scheme has distinct advantages of compactness, small power consumption and capability for integration with electronics [34, 35].

2. Optical arbitrary waveform generation

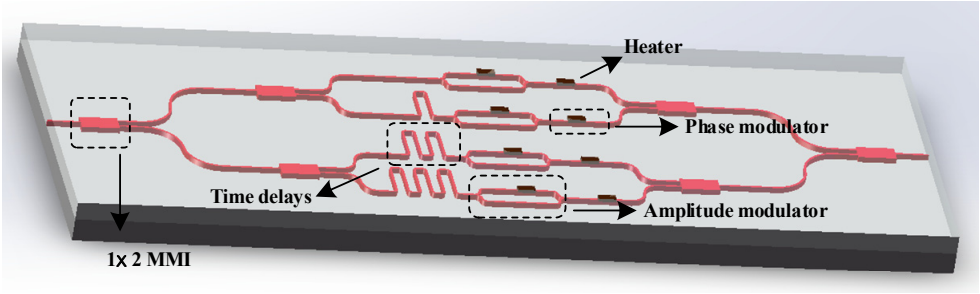

Fig. 1. Schematic diagram of the proposed on-chip pulse shaper.

The pulse shaper is based on a four-tap FIR structure. The pattern structure is monolithically integrated on an SOI wafer, with the advantages of easy fabrication and compact footprint. The pulse shaper architecture is shown in Fig. 1. The input signal is divided into four taps by cascaded multimode interferometer (MMI) couplers, and then propagates through the four taps with a series of time delays. An amplitude modulation unit (realized by a MZI with one arm phase-modulated) and a phase modulation unit are present on each tap. All phase modulation units are controlled by thermal electrodes. Assuming that the amplitudes and phases of the four taps are α_1, α_2, α_3, α_4 and ϕ_1, ϕ_2, ϕ_3, ϕ_4, respectively, and the time delay

#236566 - $15.00 USD Received 19 Mar 2015; revised 24 Apr 2015; accepted 27 Apr 2015; published 29 Apr 2015

between two adjacent taps is τ, the transfer function of the optical pulse shaper can be expressed as

$$H_0(\omega)=\sum_{n=1}^{4}\alpha_n e^{j(n\omega\tau+\phi_n)} \tag{1}$$

where ω is angular frequency of light. Equation (1) indicates that the output spectrum can be reshaped by modifying the relative amplitude weights and phase shifts of the four taps. Assuming that the relative time delay between two consecutive taps is 10 ps, a pulse shaper can be obtained with a free spectral range (FSR) of 100 GHz.

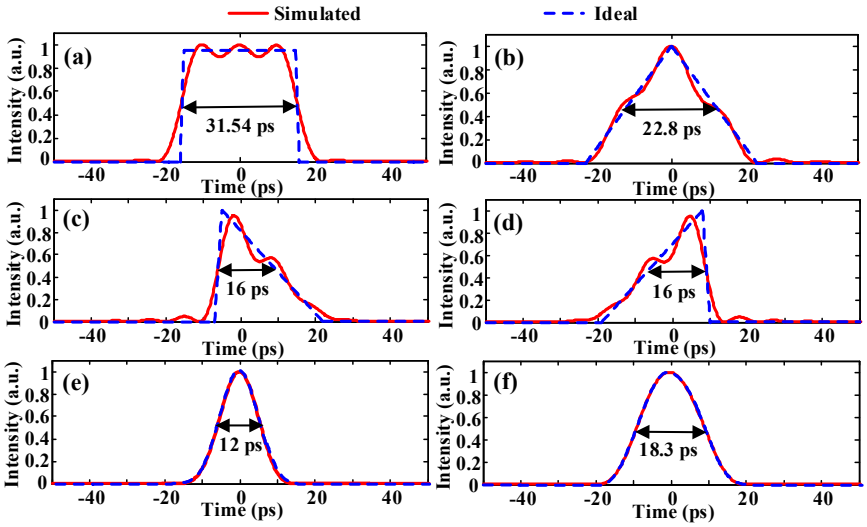

Fig. 2. Simulated waveforms (red solid line) of the pulse shaper and the ideal ones (blue dash line) of (a) square waveform (the amplitude array and phase array are [0.93, 1, 1, 0.94] and [0.305π, 0.013π, –0.015π, 0.23π], respectively), (b) isosceles triangular waveform (the amplitude array and phase array are [0.69, 1, 0.75, 0.114] and [-0.05π, –0.4π, –0.1π, –0.1π], respectively), (c) and (d) sawtooth waveforms (the amplitude array and phase array are [0.15, 0.46, 0.77, 1], [0.5π, –0.1π, –0.3π, 0.09π] and [1, 0.77, 0.46, 0.15], [0.09π, –0.3π, –0.1π, 0.5π], respectively), (e) and (f) Gaussian waveforms (the amplitude array and phase array are [0.2, 1, 0.5, 0], [0, 0, 0, 0] and [0.65, 1, 0.65, 0], [0.1π, 0, 0, 0], respectively).

Several typical waveforms can be achieved by jointly tuning both amplitude and phase arrays for all taps. The target waveform can be designed by calculating the amplitude and phase array according to Fourier transformation. Figure 2(a) shows an example of square waveform generation with the pulse shaper. The amplitude array and phase array of this case are α = [0.93, 1, 1, 0.94] and ϕ = [0.305π, 0.013π, –0.015π, 0.23π], respectively. And the simulated output waveform is shown as the red solid line. The full width at half maximum (FWHM) of the simulated square waveform is 31.54 ps. In Fig. 2(b) we set the amplitude array and phase array to α = [0.69, 1, 0.75, 0.114] and ϕ = [-0.05π, –0.4π, –0.1π, –0.1π], respectively, and we can achieve isosceles triangular waveform by this pulse shaper. The FWHM of the simulated isosceles triangular waveform is 22.8 ps. Then we simulate a sawtooth waveform by setting the amplitude and phase array to α = [0.15, 0.46, 0.77, 1] and ϕ = [0.5π, –0.1π, –0.3π, 0.09π], respectively. In order to achieve the opposite sawtooth waveform, we can just reverse the amplitude and phase array, i.e. α = [1, 0.77, 0.46, 0.15] and ϕ = [0.09π, –0.3π, –0.1π, 0.5π], respectively. The corresponding simulated waveforms are shown in Figs. 2(c) and 2(d). The FWHM of the simulated sawtooth waveform is 16 ps. By setting the amplitude and phase array to α = [0.2, 1, 0.5, 0] and ϕ = [0, 0, 0, 0], respectively, a Gaussian waveform with a FWHM of 12 ps can be achieved. The corresponding simulated

#236566 - $15.00 USD Received 19 Mar 2015; revised 24 Apr 2015; accepted 27 Apr 2015; published 29 Apr 2015

waveform is shown in Fig. 2(e). And a Gaussian waveform with a FWHM of 18.3 ps can be obtain when the amplitude and phase array are α = [0.65, 1, 0.65, 0] and ϕ = [0.1π, 0, 0, 0], respectively. The corresponding simulated waveform is shown in Fig. 2(f). Note that the amplitude and phase arrays in these cases are particularly calculated with Fourier transformation of target waveforms. The ideal waveforms of square waveform, isosceles triangular waveform, sawtooth waveforms and Gaussian waveforms are also shown in the Figs. 2(a)-2(f) (blue dash line) for comparison. The FWHMs are 30.7 ps, 23 ps, 14.5 ps, 12 ps and 18.3 ps, respectively. As shown in Fig. 2, the simulated waveforms are in good agreements with the ideal ones. Very little distortion can be found due to the loss of high frequency components. The simulated waveforms in Fig. 2 are all impulse response of the pulse shaper.

The microscopic image of the fabricated pulse shaper is shown in Fig. 3. The pulse shaper is fabricated on an SOI wafer with 250 nm thick top silicon layer and 3 μm thick buried oxide (BOX). The height of the waveguide is 250 nm and the relative time delay of the four taps is 10 ps. The bending radius of the waveguide is 20μm. The size of our pulse shaper is only 2 mm^2. Fully etched apodized grating couplers [36] are used as input and output ports. A single step of E-beam lithography and inductively coupled plasma reactive ion etching (ICP-RIE) is used to fabricate the grating couplers and silicon waveguides, simultaneously. Then a 700 nm thick silica is deposited on the sample. Another layer of 700 nm boro-phospho-silicate-glass (BPSG) is deposited annealed in nitrogen condition in order to planarize the surface. After that, the top glass layer is thinned to 1μm by buffered hydrofluoric acid (BHF) etching. Finally, heater patterns (100 nm Ti) are formed by E-beam lithography followed by metal deposition and lift-off. The on-chip insertion loss of our pulse shaper is 9 dB when there is no voltages applied to the electrodes. The loss of the coupling from the grating to fiber is about 11dB for both sides. All four taps are fabricated with metal thermal conductors to tune the amplitude and phase respectively. The insertion loss can be effectively reduced by introducing an aluminum mirror by flip-bonding process [37].

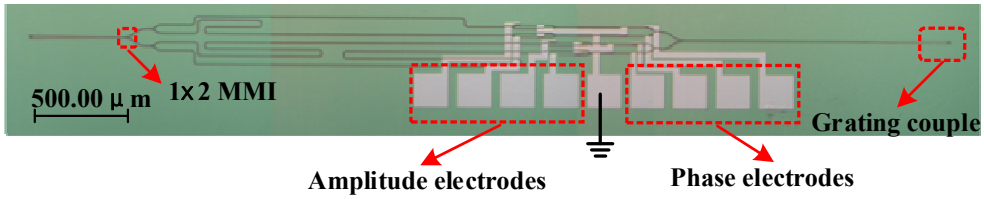

Fig. 3. Metallurgical microscopy image of the on-chip pulse shaper.

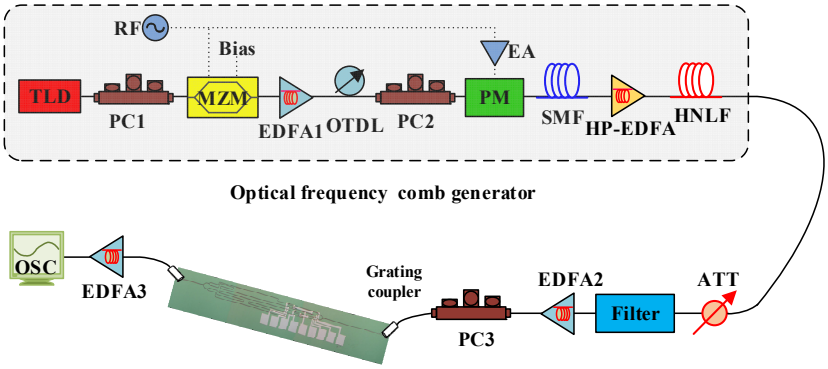

Fig. 4. Experimental setup of the arbitrary waveform generation with employing the on-chip pulse shaper.

In order to characterize our on-chip pulse shaper, we use the experimental setup as shown in Fig. 4 to generate several typical waveforms. A continuous wave (CW) light is emitted

#236566 - $15.00 USD Received 19 Mar 2015; revised 24 Apr 2015; accepted 27 Apr 2015; published 29 Apr 2015

from the tunable laser diode (TLD) with a precisely tuning resolution of 100 kHz. The light is modulated by the Mach–Zehnder modulator (MZM) and phase modulator (PM), which are driven by a tunable radio frequency (RF) signal (10 GHz ~~initially~~). Because of the polarization sensitivity, there are two polarization controllers (PCs) placed before the MZM and PM. A 5-km single mode fiber (SMF) is used to compensate the incident chirps to generate more and flatter optical frequency comb lines. A 1020-m high nonlinear fiber (HNLF) is used afterwards to increase the optical frequency comb lines by self-phase modulation. By using this optical frequency comb generator, we can achieve about 80 spectral lines at 10 GHz. Since the transmission spectrum of the pulse shaper is periodical, a tunable optical band-pass filter is used to pick out one period of the spectrum of the silicon chip. In this experiment we use two vertical grating couplers to couple the light from fiber to silicon waveguide and the output signal from waveguide to fiber. Because of the polarization sensitivity of the grating couplers, a polarization controller (PC) is placed before the input grating coupler. The electrodes of the amplitude and phase arrays are contacted by a probe pin array spaced with 250 μm. Variable voltages generated from independent power supplies are applied to different pins in the array. Finally the output temporal waveform is measured by a high speed oscilloscope (OSC) with a bandwidth of 500 GHz (Eye-Checker 1000C) and the measured waveforms are all averaged by 11.

Figure 5 shows the measured waveforms and spectra of the generated optical frequency comb (OFC) and the input signal launched into the pulse shaper. The spectrum of the OFC is shown in Fig. 5(a) as the blue solid line. A flat OFC of about 80 lines with power deviation less than 5-dB can be obtained. And the spectrum of the signal after the band-pass filter is also shown in Fig. 5(a) as the red solid line. The bandwidth of the band-pass filter is 0.8 nm. The waveforms of the OFC and input signal are shown in Fig. 5(b), and the FWHMs are 3.5 ps and 11.2 ps. The repetition rates of OFC and input signal are both 10 GHz.

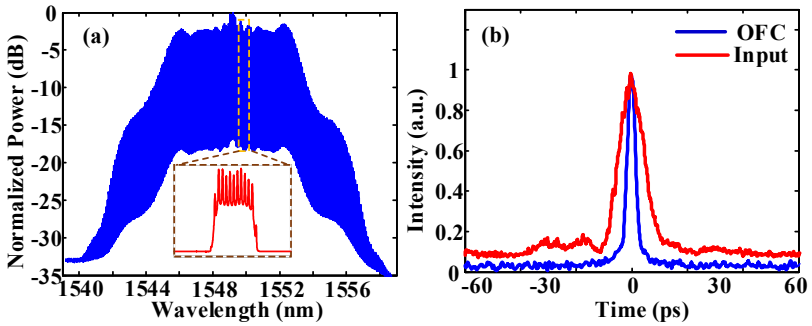

Fig. 5. (a) Measured spectra of OFC (blue solid line) and input signal (red solid line), (b) measured waveforms of OFC (blue solid line) and input signal (red solid line).

Figure 6(a) shows the measured square waveform. The FWHM of the measured waveform is 29.2 ps, and the output waveform is shown as the blue solid line. The signal to noise ratio (SNR) is 39.34 dB. To achieve this waveform, we adjust all the voltages applied on the amplitude electrodes and phase electrodes so that the output of pulse shaper matches well with the simulated condition. With similar method, we can achieve isosceles triangular waveform, which is shown in Fig. 6(b) as the blue solid line. The FWHM is 19.4 ps and the SNR is 42.51 dB. Two opposite sawtooth waveforms are shown in Figs. 6(c) and 6(d) with the FWHMs of 15.5 ps and 14.5 ps, respectively. The SNRs of the two sawtooth waveforms are 41.56 dB and 42.16 dB, respectively. The slight difference of the FWHMs may result from the unbalance power of each tap. Gaussian waveforms with the FWHMs of 12 ps and 18.3 ps are shown in Figs. 6(e) and 6(f). The SNRs are 40.25 dB and 38.17 dB, respectively. The ideal ones are also shown as the red dash line for comparison.

#236566 - $15.00 USD Received 19 Mar 2015; revised 24 Apr 2015; accepted 27 Apr 2015; published 29 Apr 2015

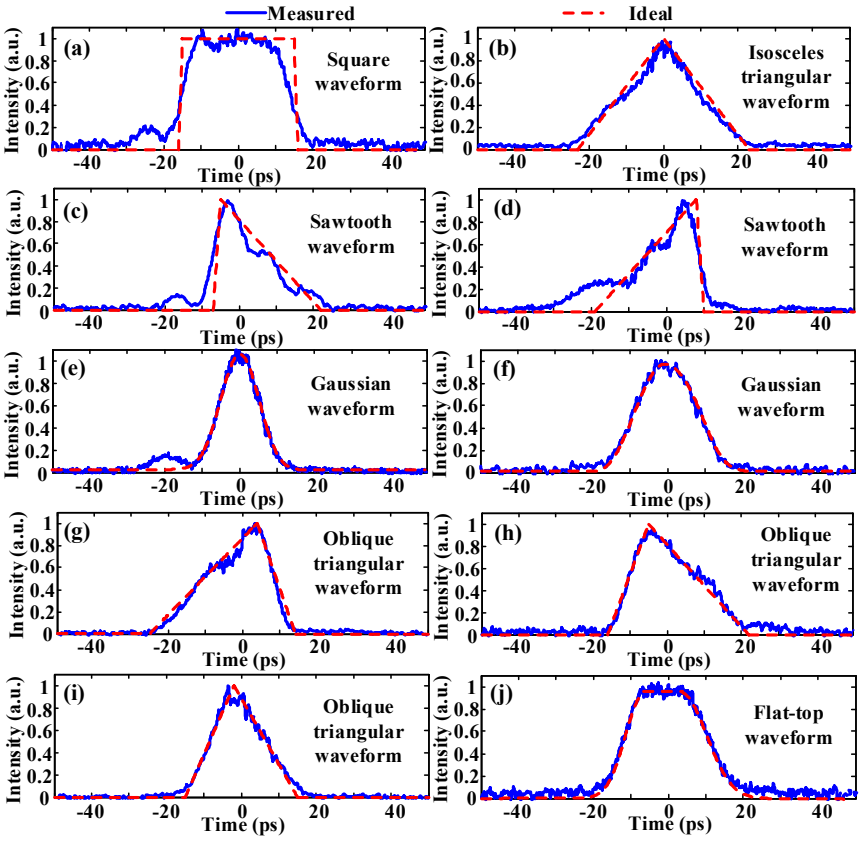

Fig. 6. Measured waveforms (blue solid line) of the pulse shaper and ideal ones (red dash line) of (a) square waveform, (b) isosceles triangular waveform, (c) and (d) sawtooth waveform, (e) and (f) Gaussian waveform, (g), (h) and (i) oblique triangular waveform, (j) flat-top waveform.

In order to demonstrate that our scheme can generate more general waveforms, we adjust the voltages controlling both amplitude and phase arrays to achieve some oblique triangular waveforms and flat-top waveform. Figures 6(g) and 6(h) are two opposite oblique triangular waveforms with the FWHMs of 19.55 ps and 20.1 ps, respectively. The SNRs of the two oblique triangular waveforms are 38.77 dB and 39.59 dB, respectively. The ideal ones are also shown as the red dash line, and the FWHMs are 19.6 ps. Figure 6(i) is another kind of oblique triangular waveform, the FWHMs of the measured waveform and the ideal one are 15.88 ps and 15 ps, respectively. The SNR of the oblique waveform is 39.19 dB. The measured flat-top waveform is shown in Fig. 6(j), the FWHMs of the measured one and ideal one are both 23 ps. And the SNR of the measured flat-top waveform is 39.83 dB. The temporal resolution of all the generated waveforms is 10 ps and the temporal window of our pulse shaper is about 40 ps. As shown in Fig. 6, the measured waveforms are in good agreements with the ideal ones, that is to say, our scheme has a good performance on waveform generation. Figure 7(a) shows the spectra of input optical frequency comb (blue solid line) and the output square waveform (black dotted line). And the spectrum of the pulse shaper is also shown as the red dash line. Figures 7(b) to 7(j) are the spectra of optical frequency comb and the output isosceles triangular waveform (7(b)), sawtooth waveform (7(c) and 7(d)), Gaussian waveform (7(e) and 7(f)), oblique triangular waveform (7(g), 7(h) and 7(i)) and flat-top waveform (7(j)).

#236566 - $15.00 USD Received 19 Mar 2015; revised 24 Apr 2015; accepted 27 Apr 2015; published 29 Apr 2015

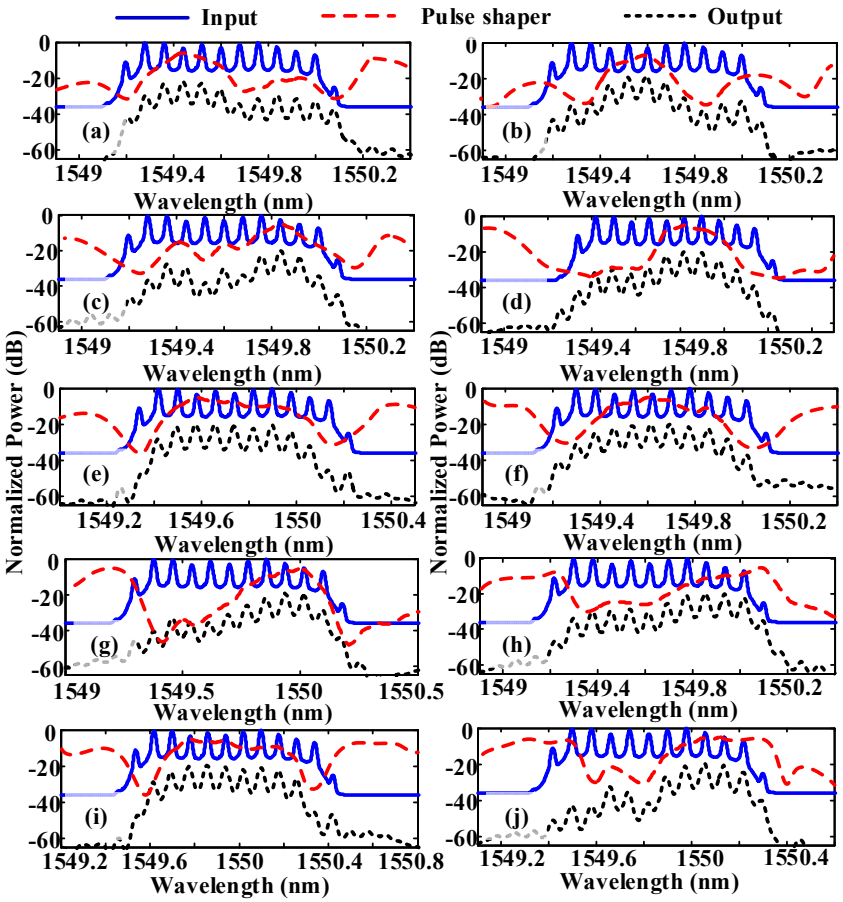

Fig. 7. Measured spectra of input optical frequency comb and output waveforms of (a) square waveform, (b) isosceles triangular waveform, (c) and (d) sawtooth waveform, (e) and (f) Gaussian waveform, (g), (h) and (i) oblique triangular waveform, (j) flat-top waveform.

3. First- to third-order differentiators

Optical differentiator attracts lots of interests due to its potential wide applications in optical analog processing [38–40], pulse characterization and ultra-high-speed coding. And it is one of the most important applications of OAWG. Here we demonstrate the first- to third-order differentiators by our pulse shaper.

Equation (1) indicates that the output spectrum can be reshaped by modifying the relative amplitude weights and phase shifts of the four taps. We can obtain a first- to third-order differentiators by controlling both amplitude and phase arrays to make sure that the transfer functions of the pulse shaper match the spectra of the first-, second- and third-order differentiators.

Figures 8(a1) and 8(a2) show the simulated amplitude response and phase response of first-order differentiator of the pulse shaper (blue solid line). Based on Fourier transformation, the amplitude and phase array are set by α = [0.0675, 1, 0.028, 1], ϕ = [-π, -π, π, –0.15π], respectively. Figures 8(b1) and 8(b2) show the simulated amplitude response and phase response of second-order differentiator of the pulse shaper (blue solid line). The amplitude and phase array are α = [0.38, 0.746, 1, 0.38], ϕ = [-0.075π, 0.13π, 0.06π, –0.025π], respectively. Figures 8(c1) and 8(c2) show the simulated amplitude response and phase response of third-order differentiator of the pulse shaper (blue solid line). The amplitude and

#236566 - $15.00 USD Received 19 Mar 2015; revised 24 Apr 2015; accepted 27 Apr 2015; published 29 Apr 2015

phase array are α = [0.18, 0.624, 1, 0.48], ϕ = [0.04π, 0.08π, 0.01π, –0.03π], respectively. The ideal ones are also shown in the Figs. 6(a1)-(c2) as the red dash line for comparison. As shown in Fig. 8, the simulated spectra are in good agreements with the ideal ones, indicating the potential of our pulse shaper to be an order-tunable differentiator.

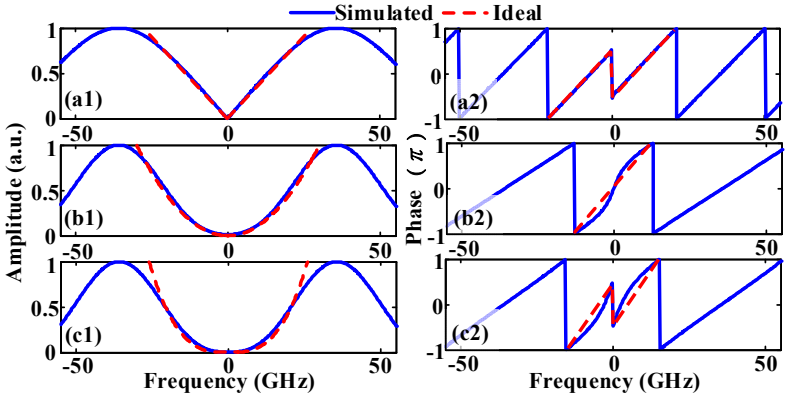

Fig. 8. Simulated amplitude-frequency responses/ phase-frequency responses (blue solid line) of the pulse shaper and the ideal ones (red dash line) of different order differentiators, (a1) and (a2) amplitude-frequency and phase-frequency responses of first-order differentiator (the amplitude array and phase array are [0.0675, 1, 0.028, 1] and [-π, -π, π, –0.15π], respectively), (b1) and (b2) amplitude-frequency and phase-frequency responses of second-order differentiator (the amplitude array and phase array are [0.38, 0.746, 1, 0.38] and [-0.075π, 0.13π, 0.06π, –0.025π], respectively), (c1) and (c2) amplitude-frequency and phase-frequency responses of third-order differentiator (the amplitude array and phase array are [0.18, 0.624, 1, 0.48] and [0.04π, 0.08π, 0.01π, –0.03π], respectively).

Figures 9(a)-9(c) show the measured spectra (blue solid line) of the pulse shaper under different amplitude and phase array conditions for the first-, second- and third-order differentiators, respectively. The ideal frequency responses (red dash line) for these differentiators are also shown for comparison. Good agreements between the ideal and the measured transfer functions are achieved in a finite bandwidth.

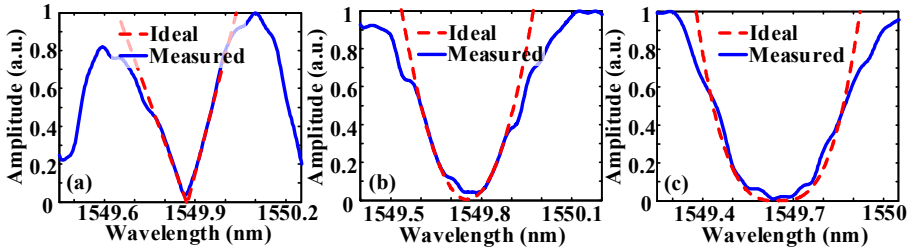

Fig. 9. Measured and ideal spectra of (a) first-, (b) second-, and (c) third-order differentiators.

The experimental setup for the first- to third-order differentiator is the same as that of OAWG, which is shown in Fig. 4. Figure 10(a) shows the spectra of input pulse (blue solid line) and the output first-order differentiation pulse (black dotted line). And the spectrum of the pulse shaper is also shown as the red dash line. We tune the central wavelength of TLD to be aligned with the resonant notch of pulse shaper. Figures 10(b) and 10(c) are the spectra of input pulses and the output second- and third-order differentiation pulses. The input signal carriers are also well aligned with the pulse shaper resonant notches. Figure 11(a) shows the input pulse generated by the optical frequency comb generator. The FWHM of the pulse is 11.2 ps. We adjust ~~the~~ all the voltages applied on the amplitude electrodes and phase electrodes to achieve a first-order differentiator spectrum, and fine tune the TLD central

#236566 - $15.00 USD Received 19 Mar 2015; revised 24 Apr 2015; accepted 27 Apr 2015; published 29 Apr 2015

wavelength to align with the resonant notch. The central wavelength of the TLD is 1549.9 nm under this condition. We measure the temporal waveforms of first-order differentiation signal, which is shown in Fig. 11(b) as the blue solid line. The SNR of the signal is 35.45 dB. Then we adjust ~~the~~ all the voltages applied on the amplitude electrodes and phase electrodes to achieve the second- and third-order differentiator spectra, still fine tune the TLD central wavelength to align with the resonant notch. The central wavelengths of the TLD are 1549.7 nm and 1549.7 nm, respectively. And we measure the temporal waveforms of second- and third-order differentiation, which are shown in Figs. 11(c)-11(d), respectively. The SNRs of the second-order and third-order differentiation signals are 34.75 dB and 34.67 dB, respectively. It can be seen that the shape of the measured differentiated pulses fit well with the simulated ones, but the pulsewidths of the measured pulses are much larger than the simulated ones. The FWHM of the measured first-order differentiation pulse is 22.54 ps, and that of the simulated one is only 17.6 ps. The pulse broadening is 28.1%. The FWHM of the measured second-order differentiation pulse is 7.2 ps, and that of the simulated one is 5.6 ps. The pulse broadening is 28.3%. The FWHM of the measured output third-order differentiation pulse is 21.22 ps, and that of the simulated one is 14.8 ps. The pulse broadening is 43.4%. The reason of this phenomenon is that the bandwidth of the input pulse is larger than the operation bandwidth of pulse shaper.

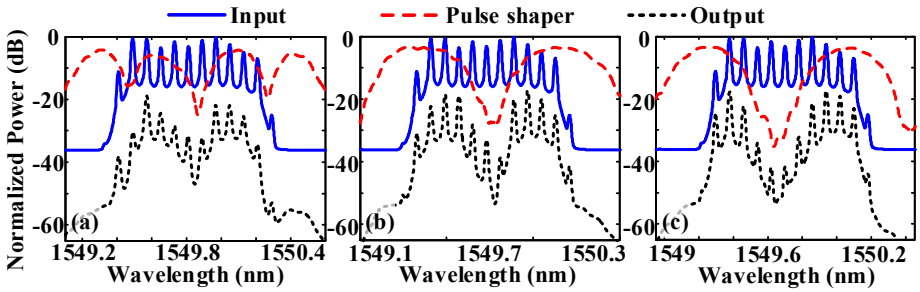

Fig. 10. Measured spectra of input pulse and output differentiation signals of (a) first-order, (b) second order, and (c) third-order.

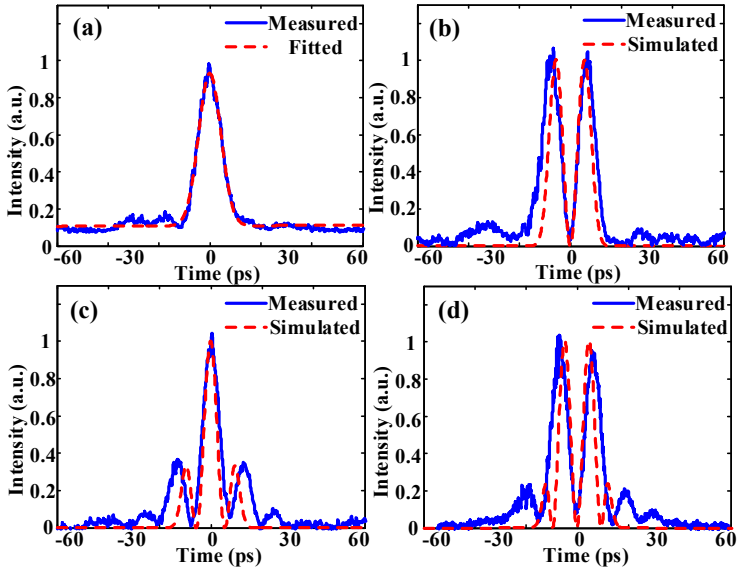

Fig. 11. Experimental results for different order differentiations, (a) input pulse, (b)-(d) temporal waveforms for first-, second- and third-order differentiations, respectively.

#236566 - $15.00 USD Received 19 Mar 2015; revised 24 Apr 2015; accepted 27 Apr 2015; published 29 Apr 2015

In order to figure out pulse broadening issue, we simulate the output pulse broadenings of input signals with different pulsewidths. Taking second-order differentiator for an example, the output pulse broadening of different input pulsewidth signal is shown in Fig. 12. In our scheme, the output differentiation pulse would not be distorted when the FWHM of the input pulse is larger than 23.5 ps. The broadening increases with the decrease of pulsewidth of the input signal, and would be almost 50% when the FWHM of the input pulse decreased to 10 ps.

In order to verify our prediction, we launch an input pulse with larger pulsewidth into the chip and measured the new output differentiation pulse. The experiment setup is shown in Fig. 13. Still a CW light is emitted from the TLD. The light is modulated by a MZM and a PM, which are also driven by a 10 GHz RF signal to generate optical frequency comb lines. But there are no SMF and HNLF in the experiment setup. So the lines are much fewer than that in OAWG experiment, resulting in a much broader input pulse. Because the bandwidth of the input spectrum (0.6 nm) is smaller than the FSR of the pulse shaper, no band-pass filter is needed. Then two vertical grating couplers couple the light from fiber to silicon waveguide and the output signal from waveguide to fiber. Because of the polarization sensitivity of the couplers and waveguides, a PC is placed before the input grating coupler.

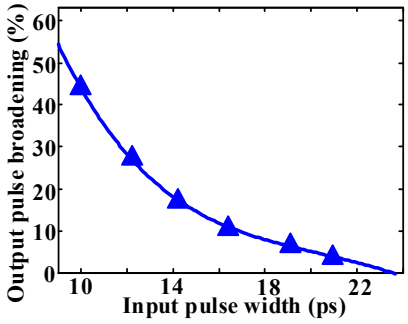

Fig. 12. Output pulse broadening with the pulsewidth of the input signal.

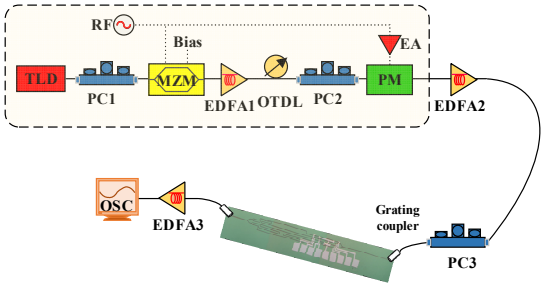

Fig. 13. Experimental setup of the different order differentiators with broader input pulse.

Figure 14(a) shows the input pulse generated by the new experiment setup. The FWHM of the pulse is 25.4 ps. We control ~~the~~ all the voltages applied on the amplitude electrodes and phase electrodes to achieve the first-order differentiator spectrum, and fine tune the TLD central wavelength to align with the resonant notch. We measure the temporal waveform of first-order differentiation signal, which is shown in Fig. 14(b) as the blue solid line. The SNR of the signal is 35.01 dB. The ideal first-order differentiation signal is also shown as the red dash line for comparison. Obviously, the output differentiation signal is not broadened. Then we adjust ~~the~~ all the voltages applied on the amplitude electrodes and phase electrodes to achieve the second- and third-order differentiator spectra, still fine tune the TLD central wavelength to align with the resonant notch. And we measure the temporal waveforms of the

#236566 - $15.00 USD Received 19 Mar 2015; revised 24 Apr 2015; accepted 27 Apr 2015; published 29 Apr 2015

second- and third-order differentiations, which are shown in Figs. 14(c) and 14(d), respectively. The SNRs of the second-order and third order differentiation signals are 24.04 dB and 23.99 dB, respectively. The output signals are not broadened, either, confirming our prediction. We may also notice that the differentiation signals have larger distortions with the ideal ones, which is caused by a low energy efficiency of photonic chip. The minimum operation frequency bandwidth of our differentiator is about 31.25 GHz, and the maximum operation frequency bandwidth is about 100 GHz (the pulse broadening is 30% for the first-order differential). And the phase at the phase jump of first- and third-order differentiators can vary with small changes of the tap's phase. So we can also achieve fractional-order differentiator by our scheme too.

The power consumption varies when the pulse shaper is in different functions, and the maximum power consumption is about 100 mW. The spectrum of the pulse shaper is periodical due to the four-tap FIR structure. The FSR of the filter is inversely proportional to the time delay τ. Thus we can increase the FSR thereafter decrease the pulsewidth of OAWG and increase the operation bandwidth of differentiator by decreasing the time delay. In practical application, the time delay τ can be 0.5 ps to 20 ps for 4 taps because of the fabrication error and large loss of the long waveguides. So the operation bandwidth of our differentiator can varies between 0.12 nm to 16 nm. Comparing the measured arbitrary waveforms and differentiation pulses with the simulations, moderate deviations appear, which result from the non-uniform thermal conductivity of each electrode and device fabrication imperfections. To mitigate the impact of thermal non-uniformities, we can increase the distance between thermal heaters to prevent thermal crosstalk. Besides, the number of taps influences the resolution of pulse shaper as well. We can obtain more elaborate waveforms by fabricating FIR structures with eight or more taps.

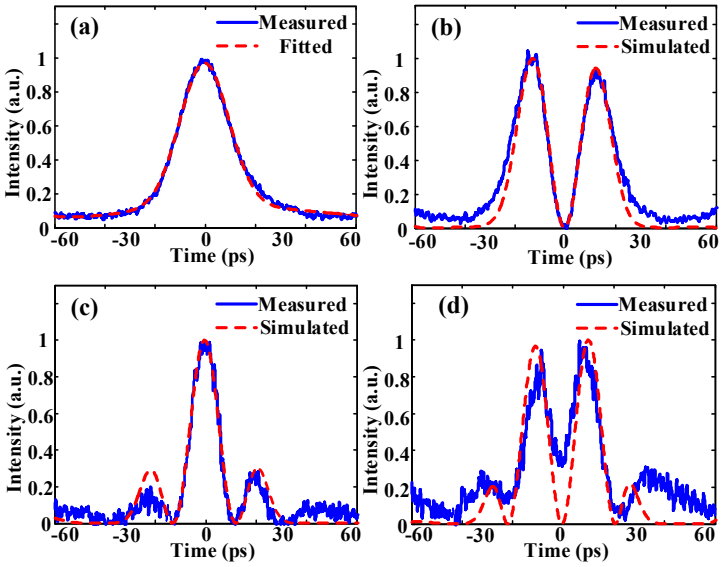

Fig. 14. Experimental results for different order differentiations of broader input pulse, (a) input pulse, (b)-(d) temporal waveforms for first-, second- and third-order differentiations, respectively.

4. Conclusions

We have proposed and demonstrated an optical arbitrary waveform generator and high-order photonic differentiator based on an FIR silicon integrated circuit. By adjusting the voltages to control the amplitude and phase of each tap, we have implement several typical waveforms such as isosceles triangular waveform, sawtooth waveform, square waveform, oblique

#236566 - $15.00 USD Received 19 Mar 2015; revised 24 Apr 2015; accepted 27 Apr 2015; published 29 Apr 2015

triangular waveform, flat-topped waveform and Gaussian waveform. And we also have demonstrated first-, second- and third-order differentiators based on the optical pulse shaper. Furthermore, we discussed the influence of the bandwidth of input pulse to a finite operation bandwidth differentiator. Our scheme has distinct advantages of compactness, small power consumption and capability for integration with electronics. And no high frequency resolution disperser or coherent detection are required in our scheme. Our scheme can achieve first- to third-order differentiator on a fixed photonic chip, which is unable in our previous schemes such as cascaded microrings or cascaded Mach-Zehnder interferometers.

Acknowledgments

This work was supported in part by the National Basic Research Program of China (Grant No. 2011CB301704), the Program for New Century Excellent Talents in Ministry of Education of China (Grant No. NCET-11-0168), a Foundation for Author of National Excellent Doctoral Dissertation of China (Grant No. 201139), the National Natural Science Foundation of China (Grant No. 11174096, 11374115, 61261130586 and 61475052), and the Opened Fund of the State Key Laboratory on Integrated Optoelectronics (Grant No. 2011KFJ002) and the Danish Council for Independent Research (DFF–1337-00152 and DFF–1335-00771).

#236566 - $15.00 USD Received 19 Mar 2015; revised 24 Apr 2015; accepted 27 Apr 2015; published 29 Apr 2015